International Journal of Hydrogen Energy 202 (2026) 152881

Contents lists available at ScienceDirect

International Journal of Hydrogen Energy

journal homepage: www.elsevier.com/locate/he

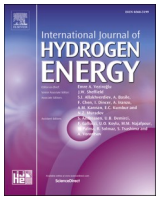

Poly(pentafluorstyrene) based ionomers for electrochemical hydrogen pumps II – Probing the electrode processes by distribution of relaxation times

M. Braig [a,b], H. Cho [c], C. Marchfelder [a,b], V. Atanasov [c], R. Zeis [a,b,d,*]

[a] Friedrich-Alexander-Universität Erlangen-Nürnberg (FAU), Faculty of Engineering, Department of Electrical Engineering, Cauerstraße 9, 91058, Erlangen, Germany
[b] Karlsruhe Institute of Technology, Helmholtz Institute Ulm, Helmholtzstraße 11, 89081, Ulm, Germany
[c] University of Stuttgart, Institute of Chemical Process Engineering, Böblinger Straße 78, 70199, Stuttgart, Germany
[d] University of Toronto, Faculty of Applied Science and Engineering, Department of Mechanical and Industrial Engineering, 5 King's College Road, Toronto, Ontario, M5S 3G8, Canada

ARTICLE INFO

Keywords:
Electrochemical hydrogen pumping
Polybenzimidazole (PBI)
PWN70
Ionomer
Electrochemical impedance spectroscopy (EIS)
Distribution of relaxation times (DRT)

ABSTRACT

The properties of different poly (pentafluorstyrene) (PPFSt) based ionomers implemented into full-cell electrochemical hydrogen pumps (EHPs) are investigated by electrochemical impedance spectroscopy (EIS) coupled with the distribution of relaxation times (DRT) analysis. Thereby, the resistances of the proton transport (PT) in the electrodes, the hydrogen evolution reaction (HER) on the cathode, the hydrogen oxidation reaction (HOR) on the anode, and the mass transport (MT) in each EHP are quantified. Phosphonated PPFSt (PWN70) ionomer exhibits superior performance with a polybenzimidazole membrane, demonstrating excellent PT and kinetics. A novel PPFSt ionomer functionalized with an imidazole group also outperforms commonly utilized PTFE binder by improving the PT and the HER, reducing the power consumption by 25 % at 1.0 A cm^{-2} and 200 °C. Both ionomers demonstrate a MT resistance comparable to the PTFE catalyst layer, caused by the high porosity of PWN70 and the high hydrophobicity of the imidazole binder.

1. Introduction

Electrochemical hydrogen pumps (EHPs) based on a phosphoric acid (PA) doped polybenzimidazole (PBI) membrane can be operated above 160 °C. Compared to EHPs with a conventional Nafion membrane, the elevated operating temperature improves the platinum catalyst's tolerance towards many hydrogen impurities like CO and H_2S. Therefore, H_2 can be separated from gas mixes with high CO contents. The higher flexibility regarding the gas feed and the low contaminant crossover makes the PBI membrane an ideal candidate for EHPs.

Commonly, polytetrafluorethylene (PTFE) is the conventional binder in combination with a PBI membrane in EHPs and fuel cells (FCs) [1–6]. Its hydrophobic properties regulate the PA distribution in the electrodes and prevent their flooding. A low PA content in the pore network improves the mass transport of the reactants, thereby improving the cell performance. Furthermore, a low amount of PA in the electrodes decreases the phosphate anion adsorption on the platinum catalyst surface, increasing its electrochemical activity. However, a certain quantity of PA must be present in the catalyst layer (CL) to conduct protons. Therefore, the PTFE content is determined by balancing good proton conductivity, fast gas diffusion, and good kinetics. Additionally, PTFE is inert and reduces the conductivity in the electrodes.

Recently, high-temperature ionomers have been developed to overcome these drawbacks [7–9]. These materials conduct protons effectively and exhibit important binder properties, like good film formation, hydrophobicity, and acid retention. Thus, a high proton conductivity and fast mass transport are accomplished simultaneously. Only a few studies on the utilization of ionomers in high-temperature EHPs exist, and these are limited to phosphonic acid ionomer binder in combination with a quaternary benzyl pyridinium poly (arylene ether sulfone) ion-pair membrane [10,11].

Several time-dependent processes determine the polarization loss of an EHP. Electrochemical impedance spectroscopy (EIS) is a valuable tool to identify and quantify each resistance. However, properly assigning

* Corresponding author. Friedrich-Alexander-Universität Erlangen-Nürnberg (FAU), Faculty of Engineering, Department of Electrical Engineering, Cauerstraße 9, 91058, Erlangen, Germany.
E-mail address: roswitha.zeis@fau.de (R. Zeis).

https://doi.org/10.1016/j.ijhydene.2025.152881
Received 1 October 2024; Received in revised form 5 November 2025; Accepted 1 December 2025
Available online 15 December 2025

impedance features to physicochemical processes is often challenging if processes overlap in the frequency domain. The distribution of relaxation times (DRT) aids in deconvoluting complex impedance spectra [12]. A quasi-assumption-free method such as DRT is advantageous for analyzing complex impedance data of electrochemical systems where a standard equivalent circuit is unknown.

While DRT provides a detailed analysis of the relaxation times, the obtained distribution yields no physicochemical interpretation, therefore, a parameter variation previously analyzed the DRT features of an EHP with a PTFE binder [3]. The proton transport (PT) in the electrodes, the hydrogen evolution reaction (HER), the hydrogen oxidation reaction (HOR), and the mass transport (MT) were identified and assigned to characteristic frequency ranges. Based on this preliminary work, the effect of different binders on each polarization loss can be quantified in a membrane electrode assembly (MEA). Ex-situ measurements, e.g. of the proton conductivity, already indicate if a material is appropriate as a binder in EHPs. However, only operando measurements reflect the complexity of practical cell operation and will ultimately determine if a polymer is a suitable candidate as an electrode binder. Therefore, investigating binders in full MEAs is crucial for analyzing the impact of the material's properties on the cell's polarization losses.

In this study, we investigate different proton-conducting binders based on poly (pentafluorstyrene) (PPFSt) in EHPs by EIS and DRT. Phosphonated PPFSt (PWN70) and novel PPFSt-Imidazolium (PPFSt-Imi) materials are employed as electrode binders in combination with a PBI membrane. The effect of Triton X-100 surfactant into the catalyst ink is studied. Furthermore, the impact of two commercial gas diffusion layers (GDLs) on the MEA behavior is evaluated. The resistances extracted from the EIS data are related to dynamic vapor sorption (DVS) and argon sorption measurements. Thus, a comprehensive analysis of each ionomer is undertaken.

2. Experimental

2.1. Binder synthesis

The synthesis and properties of the employed binders shown in Fig. 1 is described in detail in part I [13]. All binders are based on poly (pentafluorstyrene), which provides high chemical and thermal stability, and relatively high hydrophobicity. PPFSt without functionalization and PWN70 were proven to be stable up to 345 °C and 365 °C, respectively [7,14]. Functionalized PPFSt-Imi in contact with $H_2PO_4^-$ showed decomposition starting at 320 °C [14]. Thus, all polymers are suitable as ionomer in high-temeprature EHPs with operation temperatures up to 200 °C.

2.2. Membrane electrode assembly fabrication

All MEAs were based on commercial PBI membranes (Dapozol M40, Danish Power Systems) doped with 85 % PA (AnalaR Normapur, VWR Chemicals). The gas diffusion electrodes (GDEs) were fabricated by spray-coating a catalyst layer containing a 20 wt% Pt on carbon black catalyst (Alfa Aesar) onto a commercial GDL with a microporous layer (MPL). If not indicated otherwise, the Freudenberg H14CX653 GDL was utilized. The binder was varied for each GDE. Besides PTFE (60 wt% in H_2O, Sigma-Aldrich), the ionomers PWN70, PPFSt-Imi-C6, and PPFSt-Imi-C10 were employed. Furthermore, the nonionic surfactant Triton X-100 was added to the ink of the PPFSt-Imi-C10 binder where indicated. The anode and cathode in each EHP were identical and always had a catalyst loading of 1 mg Pt cm^{-2}.

The cell compression was determined by PTFE and PEEK gaskets between the membrane and each GDE. The endplates were made of stainless steel. A more detailed description of the GDE fabrication, the cell setup, and the assembly can be found in part I [13].

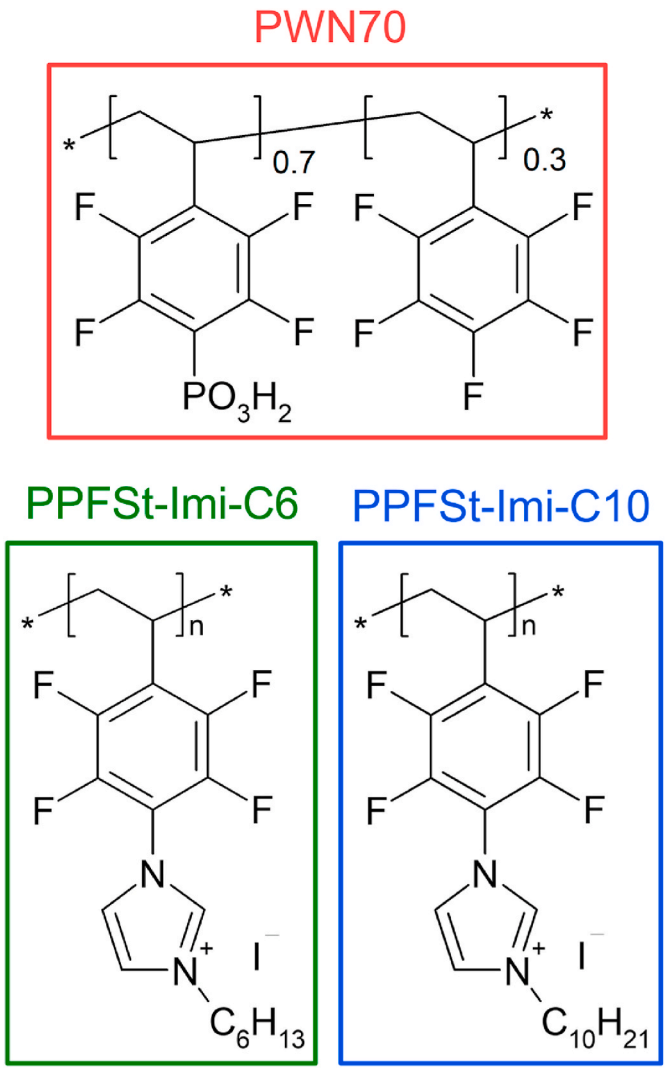

Fig. 1. Chemical structure of the investigated ionomers.

2.3. Electrochemical characterization

All cells were operated in a custom-built test station. Details on the setup and the cell conditioning process (48 h) can be found in part I [13]. No gas flow was supplied on the cathode, and neither the anode nor the cathode was pressurized.

All EHPs were characterized using EIS and potential curves (PCs) with 35 % H_2 + 1 % CO + 64 % CO_2 gas feed at 0.7 % relative humidity (RH) and $\lambda_{H2} = 2.0$, except where indicated otherwise. After adjusting the cell temperature, the EHP was operated for at least 12 h before any measurements to ensure stable cell conditions.

The electrochemical impedance spectra were recorded with a Zennium pro (Zahner Elektrik) potentiostat over the frequency range from 200 kHz to 100 mHz at various current densities with an amplitude of 25 mA cm^{-2}. Before each measurement, constant conditions were held for 30 min to ensure the system's stability. The CO in the feed gas destabilizes the cell voltage, complicating the recording of high-quality impedance spectra. EIS has to be recorded at a stable operating point. Otherwise, changing cell resistances disturbs the impedance data, which leads to erroneous interpretations [12]. Therefore, the cell voltage fluctuation must be minimized during EIS measurements. Since increased gas availability stabilizes the EHP voltage, all impedance spectra were recorded at $\lambda = 2.0$. The membrane resistance was determined from the high frequency x-axis intercept of the Nyquist plot.

The power efficiency is calculated with the flow of the evolved H_2 at

the cathode ($F_{H2,out}$), the supplied H_2 flow on the anode ($F_{H2,in}$), the heat of combustion of H_2 ($\Delta H_{combustion}$, 142 MJ kg^{-1}), and the power consumed by the EHP ($P_{applied}$).

$$\text{Power efficiency} = \frac{F_{H_{2,out}}\ \Delta H_{combustion} - P_{applied}}{F_{H_{2,in}}\ \Delta H_{combustion}} \quad (1)$$

2.4. Distribution of relaxation times

The EIS measurements were transformed into a DRT using the Relaxis3 software (rhd instruments). Only data below 100 kHz were considered since inductivity disturbed the measurement at higher frequencies. The regularization parameter was fixed to 10^{-3} as described in Ref. [3]. From the DRT, the proton transport in the electrodes, the charge transfer, and the MT resistances were extracted by integrating the area under the respective peak.

2.5. Gas sorption

Argon sorption isotherms were recorded at 87 K with an autosorb iQ (3 P Instruments) to investigate the morphology of the fabricated GDEs. The pore volume of the CL was determined by quench solid density functional theory (QSDFT) calculations. A Brunauer-Emmett-Teller (BET) surface area was calculated from the same isotherms. Details on the measurements and the data evaluation can be found in part I [13]. The GDL was also measured to subtract the sorption on the GDL from the measured GDE. As both components are weighted during the CL coating, only the CL's surface area and pore size distribution can be extracted when the GDE is measured. Thus, the binder influence on the morphology can be determined in the same GDE implemented into the EHP. This paper's pore volumes and surface areas correspond only to the CL, not the entire GDE.

2.6. Dynamic vapor sorption

Water sorption isotherms were recorded in a Q5000SA sorption analyzer (TA Instruments). The GDEs and the as-received GDL were cut into small pieces. Subsequently, the vapor adsorption and desorption were performed at 25 °C up to 90 % RH. More details on the procedure can be found in part I [13]. The sorption of the GDL was subtracted from the GDE sorption with a reference measurement. Therefore, the presented water uptake only represents the sorption of the CL, not the entire GDE.

3. Results and discussion

Fig. 2 presents an exemplary impedance spectrum, the corresponding DRT, and the reconstruction of this DRT into the Nyquist plot. Since the DRT reconstruction and the measured data are in good agreement, the DRT represents the features of the measurement well. Furthermore, this demonstrates the appropriate selection of the regularization parameter [15]. The underlying processes were assigned to each DRT peak as described in Ref. [3], and their resistances are schematically indicated in the Nyquist plot as RC elements to visualize the corresponding values.

A detailed characterization of the morphological characteristics and the hydrophobicity of the CLs containing different binders can be found in part I [13]. These results are shortly summarized in the following to facilitate the reading of this publication since the electrochemical results presented here in part II will be linked to the electrode characteristics described extensively in part I. Important morphological properties and information about the hydrophobicity of all CLs are presented in Table 1.

Scanning electron microscopy (SEM) identified an exceptionally homogenous structure of the PTFE and PWN70 based electrodes. The PPFSt-Imi ionomers resulted in an uneven CL surface, but adding Triton

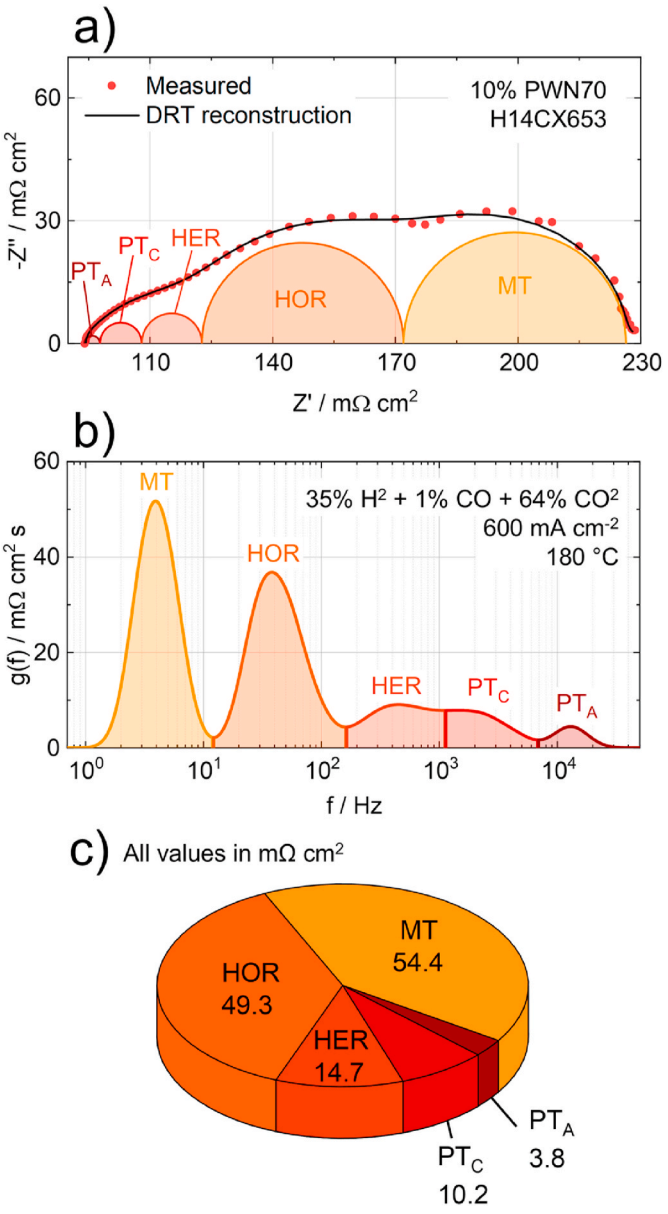

Fig. 2. a) Exemplary EIS data (red points) measured in an EHP with the GDE containing 10 % PWN70 and a Freudenberg H14CX653 GDL, and b) the corresponding DRT. The Nyquist plot reconstructed from the DRT (black line in a) shows a good agreement with the recorded data. c) The resistances were quantified by integrating the area under the respective DRT peak. (For interpretation of the references to colour in this figure legend, the reader is referred to the Web version of this article.)

X-100 surfactant into the catalyst ink significantly improved the homogeneity of the corresponding CL. However, some inhomogeneities remained, and this CL was not as evenly structured as the ones containing PTFE and PWN70.

Energy-dispersive X-ray spectroscopy (EDX) revealed an excellent binder distribution for all ionomers. However, few agglomerates with a diameter up to 10 µm were detected in the PTFE catalyst layer. The interaction between the ionomer, the electrocatalyst, and the catalyst ink solvent is critical for fabricating a homogenous CL [16–19]. Since PTFE shows minimal interaction with the solvents of the ink, the formation of agglomerates in the ink, and subsequently the CL, is unavoidable [4,20].

Argon sorption was employed to quantify the pore network in the CLs. The BET surface area and the pore volume determined by QSDFT of

Table 1
Morphological properties and hydrophobicity of the CLs containing different binders [13].

Binder	CL homogeneity	Binder distribution	BET surface area m^2 g^{-1}	Pore volume cm^3 g^{-1}	Water uptake[a] wt%
PTFE	✓	(✓)	124	0.14	5.4
PWN70	✓	✓	210	0.19	6.4
PPFSt-Imi-C10	x	✓	66	0.07	2.4
PPFSt-Imi-C10 + Triton X-100	(✓)	✓	79	0.09	3.4
PPFSt-Imi-C6	x	✓	95	0.10	3.9

[a] At 90 % RH and 25 °C.

CLs containing PWN70 and PTFE binders were higher compared to those of PPFSt-Imi based CLs. Primarily, the PWN70 binder produced highly porous and homogenous CL structures. PPFSt-Imi led to the least porous catalyst layer, but adding Triton X-100 surfactant into the catalyst ink increased both the surface area and the CL pore volume. This result is in a good agreement with the already documented improvement in the structure and performance of FC electrodes prepared using Triton X-100 [21,22].

The PWN70 CL showed the lowest hydrophobicity due to its high concentration of polar groups (Ion exchange capacity, IEC = 2.4 mmol g^{-1}). The very hydrophobic properties of the PPFSt-Imi-based CLs are caused by the relatively homogenous binder distribution within this CL. Although highly hydrophobic, PTFE leads to a less hydrophobic CL. It only adds to the hydrophobicity of the CL structure, if it is exposed in the pore network. However, a significant amount of PTFE is bound in larger agglomerates with up to 10 μm in diameter. Hence, the main part of the material is buried inside the agglomerates and thus it cannot contribute to improve the hydrophobic properties of the CL.

Fig. 3 presents the PCs of all investigated EHPs at 180 °C and 200 °C. PCs with unfilled symbols were corrected for membrane resistance. This remaining overpotential represents the combined polarization losses of the anode and the cathode.

At 180 °C, the PWN70 ionomer clearly showed the best performance. At 1.0 A cm^{-2}, PWN70 reduces the EHP voltage by 69 mV compared to the PTFE binder, corresponding to a 24 % reduction in power consumption. The PPFSt-Imi-C10 GDE prepared with Triton X-100 performed similarly to the PTFE-based MEA up to 0.8 A cm^{-2}. However, its voltage increased significantly at 1.0 A cm^{-2}, which points to hampered MT. The power consumption of the PPFSt-Imi-C10 EHP without surfactant is 43 % higher at 1.0 A cm^{-2}, highlighting the pronounced effect of Triton X-100. Furthermore, the PPFSt-Imi containing a C6 chain performs similar to the C10 version.

At 200 °C cell temperature, the MEAs with PTFE and PWN70 show slight performance improvements of 11 mV and 14 mV at 1.0 A cm^{-2}, respectively, compared to 180 °C. At higher temperatures, CO desorption becomes favored. Reducing the Pt catalyst's CO poisoning increases the electrochemically active surface area (ECSA), minimizing the kinetic resistances. The PPFSt-Imi-C10 + Triton X-100 EHP showed a more pronounced voltage decrease of 108 mV, or 34 % at 1.0 A cm^{-2} compared to 180 °C. At 200 °C, this MEA exhibited the lowest electrode resistance, as represented by the PC corrected for the membrane resistance. Thus, the PPFSt-Imi-C10 ionomer performs excellent in an EHP, but only at relatively high temperatures.

EIS was recorded to gain a deeper understanding of the electrochemical behavior of the examined binders. Fig. 4 presents EIS and DRT data of all cells collected at 600 mA cm-2. The total resistance decreases at a higher operating temperature in all EHPs, which is in accordance with the reduced slopes of the PCs shown in Fig. 3.

The electrode processes dominate the cell resistance at 180 °C, while the membrane resistance negatively impacts the EHP performance. At 200 °C, the electrode resistances decrease due to improved kinetics and the reduced adsorption of CO on the Pt catalyst. The membrane resistance is not strongly affected by the temperature increase. Although proton conductivity typically improves at higher temperatures, the loss of PA from the PBI polymer matrix at higher temperatures counteracts this effect [23]. Thus, the membrane resistance has an increased influence on the EHP behavior at higher temperatures.

The proton conductivity of PBI strongly depends on its PA doping level [24]. Since the binder in the CL regulates the PA migration from the PBI membrane into the electrodes, the electrode binder influences the membrane doping level and resistance. Therefore, the membrane resistance is different in the examined MEAs, although the identical membrane was employed in all EHPs. The correlation between the electrode hydrophobicity and the membrane resistance is described in detail in part I [13].

Fig. 5 shows the dependency of the PT within the electrodes on the temperature. All values were extracted from the DRTs displayed in Fig. 4. The cathode PT is challenging to determine since it often overlaps with the HER charge transfer resistance in the DRT. Therefore, only the anode PT resistance (PTA) was chosen for a more accurate investigation of the electrode PT resistance. The PT in the cathode likely behaves similarly.

PA increasingly dehydrates at higher temperatures, forming polyphosphates with significantly lower conductivity [25,26]. Furthermore, the proton conductivity in the CL decreases due to PA evaporation, which starts playing a role around 200 °C [7]. Since only liquid PA conducts protons in the CL with PTFE binders, both effects cause a worse PT in the GDE at higher temperatures.

The PWN70 MEA exhibits the best proton conductivity over the entire investigated temperature range between 160 and 200 °C. The PT resistance increases slightly from 160 to 200 °C due to the dehydration

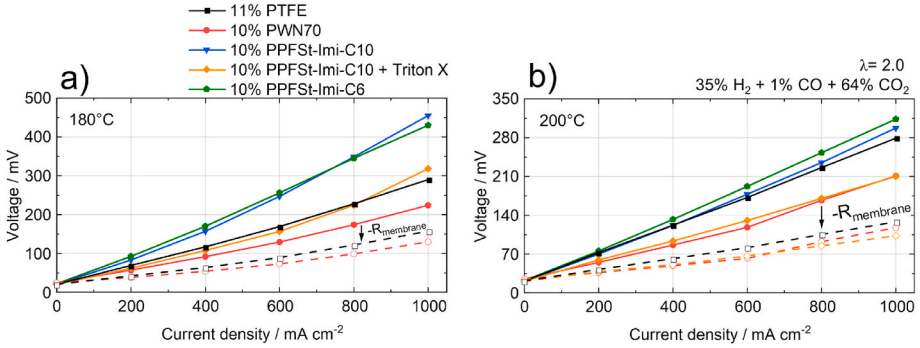

Fig. 3. EHP polarization curves at a) 180 °C, and b) 200 °C. All measurements were conducted with 35 % H_2 + 1 % CO + 64 % CO_2 gas feed at λ = 2.0 and 0.7 % RH.

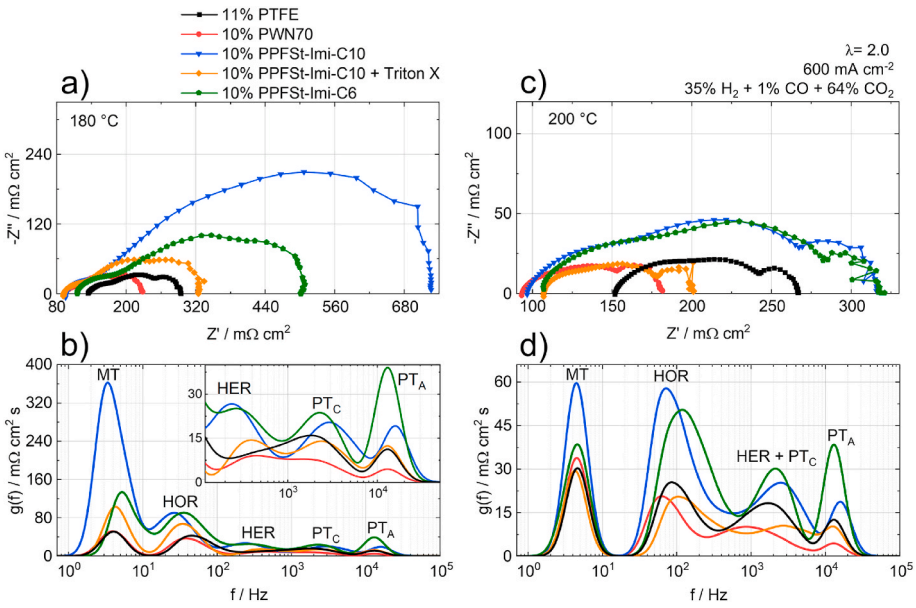

Fig. 4. EIS at 600 mA cm^{-2} recorded at a) 180 °C, and b) 200 °C. c) and d) the corresponding DRTs with an enlarged section of the high-frequency data. All measurements were conducted with 35 % H_2 + 1 % CO + 64 % CO_2 gas feed at λ = 2.0 and 0.7 % RH.

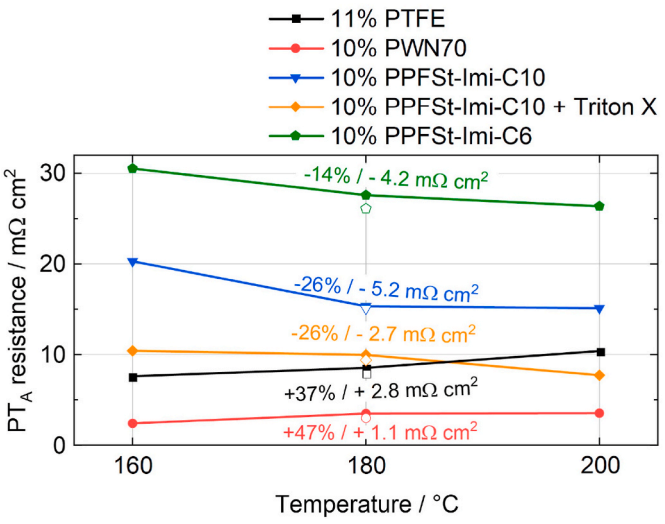

Fig. 5. Anode PT resistance dependency on the operating temperature. At 160 °C, the resistance was extracted at 100 % H_2 gas feed, while at 180 °C and 200 °C, the EIS was recorded with 35 % H_2 + 1 % CO + 64 % CO_2. The additional void symbols at 180 °C were determined at 100 % H_2, proving that the gas feed has no significant impact on the PT.

and evaporation of free PA. However, the increase is considerably lower compared to the PTFE-based MEA. The ionomer maintains a high conductivity since the bonding of PA to the phosphonic acid groups of the polymer reduces dehydration and evaporation. Stable operation of PWN70 electrodes at 200 °C was already demonstrated in a FC, suggesting that PWN70 maintains a good conductivity at higher temperatures [7]. Our findings are in accordance with these results.

The PT improved significantly at higher temperatures in all MEAs with a PPFSt-Imi binder. For the PPFSt-Imi-C10 binder with and without surfactant, a considerable resistance reduction of 26 % was measured from 160 to 200 °C. MEAs with these binders only reach full conductivity over 160 °C. Thus, PPFSt Imi binder electrodes should be combined with more thermally stable ion-pair membranes to reach their full potential. PPFSt-Imi was expected to show a higher conductivity with the shorter C6 chain than the C10 version since it exhibits a higher concentration of active groups. However, PPFSt-Imi-C10 shows a lower PT resistance. The better PT in PPFSt-Imi-C10 might be caused by an improved PA distribution in the CL, or a different pore structure. This behavior will be the scope of further studies.

Fig. 6 presents the membrane resistances, the PT in the cathode (PT_C) and the HER, the HOR, and the MT at 180 and 200 °C. All values were extracted from the DRTs in Fig. 4. At 180 °C, EIS determined the lowest PT, HER, and HOR resistances for the PWN70 MEA, and its MT resistance is comparable to the PTFE cell. The significantly lower total electrode resistance (16 % at 0.6 A cm^{-2}, 180 °C compared to PTFE) of the PWN70 MEA determined by EIS is evident in the lower overpotential in the PC shown in Fig. 3a corrected for the membrane resistance. The EIS data of the PPFSt-Imi-C10 MEA with surfactant confirm the higher MT resistance as the reason for the increasing slope of the PC at high currents at 180 °C (see Fig. 3a). However, the PT and HER resistances are similar to those of the PTFE-based cell (see Figs. 5 and 6b). Compared to the isolating PTFE, the PPFSt-Imi binder was expected to improve the PT within the electrodes due to its interaction with PA. The improved PT at increasing temperature discussed above indicates PPFSt-Imi-C10 as proton conducting, although both MEA exhibits similar proton conductivity. These results suggest that a combination of uneven ionomer film formation and a low PA content in the electrode, indicated by the more hydrophobic CL compared to PTFE (see Table 1), counteract the PT improvement caused by the ionomer's conductivity. The HOR resistance is significantly higher than the PTFE binder-based cell, further pointing to a low triple phase boundary (TPB) caused by the poor binder film and the lower electrode homogeneity.

Since the PWN70 CL is the least hydrophobic, it contains the highest amount of PA in the electrode. A high PA content typically correlates with a sluggish MT, since the hydrogen diffusion is slower in PA than in the gas phase. However, this relationship does not seem to hold up for the PWN70-based CL. The interaction between the phosphonate groups of the ionomer and the liquid PA appears to substantially improve the PA distribution within the GDE, allowing fast gas diffusion through the pore network. Furthermore, the CL exhibits the highest porosity of all prepared GDEs (see Table 1), enhancing the MT. This correlation will be discussed in detail later in Fig. 7. The excellent PA distribution of PWN70 is also indicated by the highest proton conductivity of all examined CLs, which is further supported by the intrinsic proton

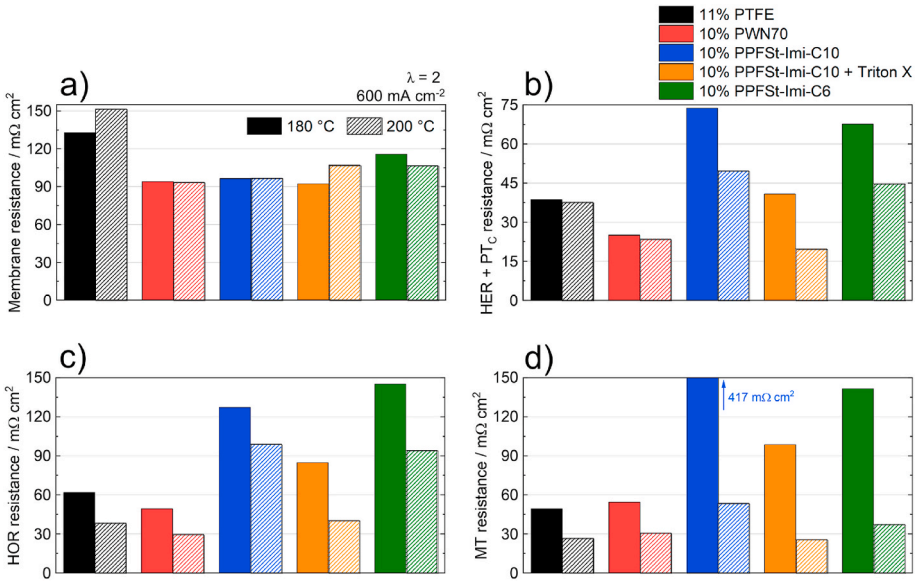

Fig. 6. Resistances of a) the membrane, b) the combined cathode PT and HER resistance, c) the HOR resistance, and d) the MT resistance for different binders at 180 °C and 200 °C at 600 mA cm^{-2} and 35 % H_2 + 1 % CO + 64 % CO_2 gas feed. The values were extracted from the data presented in Fig. 4.

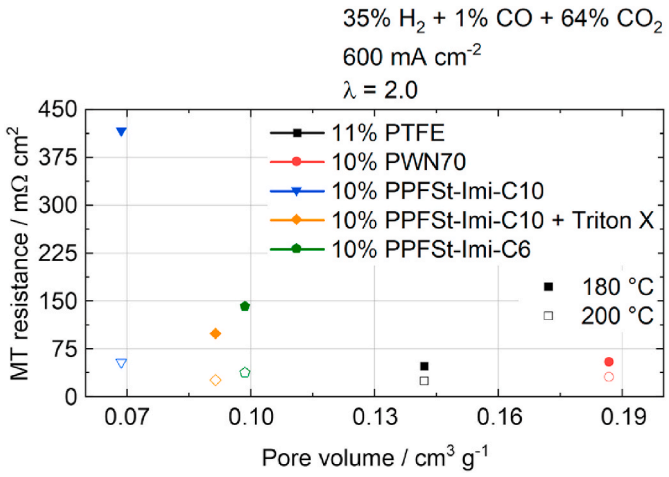

Fig. 7. Mass transport resistances determined by EIS and DRT with 35 % H_2 + 1 % CO + 64 % CO_2 gas feed at 600 mA cm^{-2} correlated with the catalyst layer pore volume determined by argon sorption (see part I [13]).

conductivity of PWN70. The presence of PWN70 in the CL also produces a low membrane resistance, likely caused by reduced interfacial resistances between the membrane and the GDEs due to the high homogeneity of the electrode.

Utilizing PWN70 also improves the HER and HOR kinetics compared to PTFE binder. The immobilization of PA on the PWN70 binder might reduce the PA in contact with Pt, decreasing the phosphate anion adsorption on the Pt surface. Thereby, the active catalyst area increases, and thus the kinetics improve. Furthermore, the phosphonate groups of PWN70 located near Pt might poison the catalyst less than liquid PA, since the binder exhibits a lower concentration of acid groups. CO desorption becomes favored at higher temperatures, decreasing the Pt catalyst's CO poisoning. This effect is evident in the decrease of the anodic HOR and MT resistances in Fig. 6. Only a minor improvement of the HER kinetics is measured for the PWN70 and PTFE MEAs. For the PPFSt-Imi-C10 + Triton X-100 MEA a higher HOR resistance and a similar HER resistance at 180 °C indicate no improvement of the kinetics compared to PTFE. However, at 200 °C, the PT improvement at higher temperatures also enhanced the charger transfer kinetics, which was apparent in the pronounced decrease of the HER and HOR resistances. The effect of the temperature on the HOR resistance seems to go beyond the desorption of CO of the Pt catalyst in the case of this ionomer since the reduction is significantly higher compared to the PTFE and PWN70 binders. The PT and the charge transfer are often highly coupled processes [27,28]. Therefore, a low PT in the vicinity of the Pt particles impedes the charge transfer, resulting in high resistances at 180 °C. At 200 °C, the improved PT leads to a pronounced reduction of the kinetic HOR and HER resistances. Furthermore, the higher catalyst availability also decreases the MT resistance.

The hydrophobic PTFE CL exhibits a good MT (see Fig. 6d), as an optimized PTFE content allows efficient gas permeation due to a low PA concentration [4]. The MT is further enhanced by a relatively high pore volume (see Table 1) of the PTFE CL. However, the isolating PTFE particles interrupt the PA film across the carbon network in the electrode, reducing the protonic and electric conductivity. Furthermore, PTFE partly covers the Pt particles, reducing the TPB. Thus, the PTFE MEA exhibits higher kinetic and PT resistances than the PWN70-based cell, since PWN70 supports proton transport in the CL and enlarges the TPB.

The PPFSt-Imi binders performed significantly worse without the surfactant. Their low electrode homogeneity reduced the TPB, which increased the kinetic resistances. Furthermore, the inhomogeneous CLs led to an inhomogeneous PA distribution, impeding the PT. The measured high MT resistance can be assigned to the considerably lower electrode porosity than that of the CL with PTFE or PWN70 binder (see Table 1). However, all these drawbacks are only caused by the bad CL morphology. Despite of that, the proton conductivity of PPFSt-Imi shows the potential of this material, making it suitable for EHP electrodes. The latter was proven with the enhanced performance observed after structural improvements achieved by employing surfactant in the catalyst ink. Furthermore, the high hydrophobicity of PPFSt-Imi makes it highly suitable as a binder in combination with a PBI membrane. Different solvent compositions or blending with other ionomers might further improve the performance.

The PPFSt-Imi + Triton-X-100 MEA showed the lowest electrode resistances at 200 °C, evident in the PC corrected for the membrane resistance (see Fig. 3b). At 200 °C, the HOR and MT resistances of the GDEs with PWN70, PTFE, and the PPFSt-Imi-C10 + Triton X-100 are similar, although the PWN70-based GDE showed a slightly lower HOR and a marginally higher MT resistance. The main reason for the better

performance of the ionomers over PTFE is related to a decrease in the cathode resistances. The proton-conducting groups seem to especially promote the HER. Apparently, the PT and the HER are linked, so the improved proton conductivity in the CL provided by the ionomers also improved the kinetics.

In combination with a PBI membrane the PWN70 CL outperforms the commonly employed PTFE-based CLs in all aspects, except for MT resistance, which is similar for both EHPs. In contrast, the PWN70/PBI combination performed worse than PTFE/PBI in an FC [7]. Since oxygen diffusion in an FC is significantly slower than hydrogen diffusion in the EHP, mass transport plays a more prominent role in FCs. The PWN70/PBI exhibits a high PA content in the electrodes since PBI and PA exhibit a relatively low intermolecular interaction energy [29]. Thus, PBI releases a high amount of PA into the electrodes, further intensified by the relatively hydrophilic properties of PWN70. The high PA content in the GDEs improves the PT but worsens the MT, reducing the overall FC performance. In EHPs, the improved PT and kinetics dominate the performance, while the MT is the major influence on the performance of polymer electrolyte membrane FCs. These findings indicate that EHPs perform optimally at higher PA concentrations than FCs. Therefore, the PWN70/PBI combination is suitable for EHPs applications. For comparison, in FCs, the PWN70 binder performs better with ion-pair membranes exhibiting higher PA binding energies. Using such systems results in significantly reduced release of PA into the GDEs and hence facilitates the MT through the electrodes [7,30].

Fig. 7 presents the MT resistance correlated to the pore volume of the corresponding CLs. An increased pore volume provides a more extensive network for gas diffusion, allowing reactants to access active sites and promoting efficient EHPs. While this correlation is generally observed for the prepared CLs, their homogeneity, PA distribution, and intrinsic conductivity also play a crucial role. For instance, an uneven electrode structure is expected to lead to local variations in the MT resistances, potentially reducing the cell performance. Since the PPFSt-Imi-C10 + Triton X-100 MEA exhibits a more homogenous CL than the PPFSt-Imi-C6 CL, it provides improved gas diffusion despite its lower pore volume. On the other hand, the PWN70 MEA shows the highest pore volume by far, but it also contains the most PA in the CL due to the comparably low binder hydrophobicity. The higher PA uptake counteracts the excellent porosity, causing MT resistance similar to the less porous PTFE MEA. While porosity plays an apparent role in gas diffusion, this is only one influence among several CL properties playing important role in the performance of EHPs. The multidimensional nature of MEA design and the comprehensive understanding of these interactions has to be achieved.

The GDL plays a vital role in the EHP performance by influencing the PA distribution in the MEA. Its MPL poses a barrier for the PA electrolyte, thereby preventing the leaching of PA. For PA-doped PBI membranes, relatively dense MPLs with a high polymer content are typically employed [31,32]. The comparably low porosity of these layers also poses a diffusion barrier for the reactant gases, inhibiting the MT in the MEA [33]. Therefore, a trade-off between good MT and low PA permeation through the MPL has to be accepted. Furthermore, the interfacial resistances of CL/MPL and GDL/flow field depend on the chosen GDL.

In this study, two commercial Freudenberg GDLs with MPL were employed. H14CX653 contains a very hydrophobic MPL with low porosity based on carbon fibers subjected to a hydrophobic treatment [34]. H23C2 exhibits a more porous but less hydrophobic MPL with an untreated carbon fiber support. The water sorption behavior of both GDLs is presented in Fig. 8. The lower water uptake for the H14CX653 GDL demonstrates its higher hydrophobicity, which reduces the PA migration from the MEA through the GDL into the flow field.

Fig. 9 presents PCs, electrochemical impedance spectra, and the corresponding DRTs of EHPs with both GDLs, each with an identical CL containing a 10 % PWN70 binder. The PWN70/H23C2 MEA demonstrated the best performance of all tested EHPs. The main reason for the

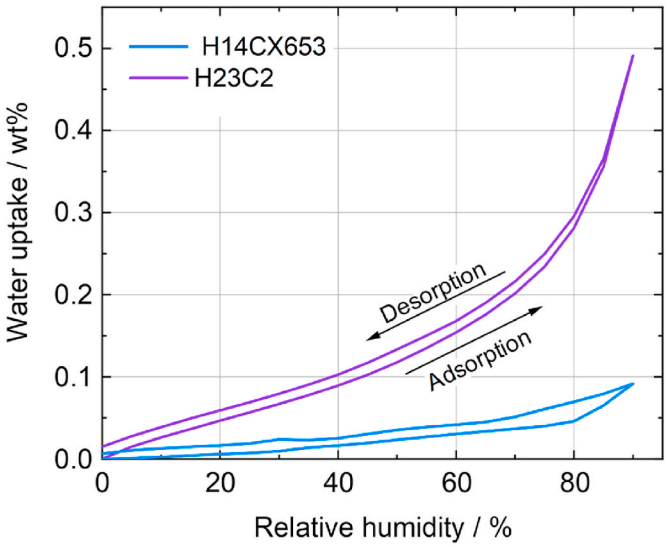

Fig. 8. Water vapor sorption isotherms of pristine GDLs measured at 25 °C.

better performance is the lower high-frequency resistance, which represents the MEA's conductivity. The coating of the highly hydrophobic H14CX653 GDL is challenging, which causes a higher interfacial resistance between the CL and the MPL.

The PC corrected for the high-frequency resistance performs better for the H23C2 GDL, suggesting lower electrode resistances. The EIS and DRT data indicate worse PT and kinetics but a better MT for the EHP with a H23C2 GDL. The H14CX653 MPL contains more PA in the MEA due to its hydrophobic properties, which improves the PT and the kinetics on the anode and the cathode. In a previous study, an improvement of the HER kinetics was also measured when the conductivity in an MEA containing PTFE binder was increased by a higher RH. Still, no influence on the HOR could be detected [3]. An improved protonation of the PWN70 binder by a higher PA content might increase the TPB. Pt catalyst covered by the ionomer increasingly becomes available as a higher protonation facilitates the H^+ transport through the film.

The H23C2 GDL decreases the MT resistance by 8 % due to its higher MPL porosity than the H14CX653 GDL. Furthermore, the lower hydrophobicity of the H23C2 GDL causes more PA leaching out of the MEA. The resulting lower PA content in the CL also improves the MT. Since the MT dominates the EHP performance at very low stoichiometry, the H23C2 cell performed exceptionally well at $\lambda = 1.0$. Thus, choosing a suitable GDL is essential for high-performing EHPs. A good diffusion process is vital for gas feeds with relatively low H_2 concentrations, making the H23C2 GDL suitable for the employed PWN70/PBI combination at the set gas feed. Especially at high current density, the H23C2 MEA retained a high efficiency.

4. Conclusions

EIS, combined with the DRT method, analyzed the impact of different binders on the polarization losses of EHPs. It is a powerful tool for investigating the morphological and physicochemical effects on cell performance. Together with the results of part I, this study describes a comprehensive approach to evaluating ionomers.

Different proton-conducting ionomers and PTFE were tested in MEAs. All investigated ionomers possess a poly (pentafluorstyrene) backbone, which was either partially phosphonated (PWN70) or connected to an imidazole group (PPFSt-Imi). The hydrophobicity of PPFSt-Imi was enhanced with an alkyl chain (C_6H_{13} or $C_{10}H_{21}$) at the imidazole. EIS and DRT analysis were employed to investigate the proton transport in the electrodes, the HER and HOR charge transfer, and the MT. All resistances were quantified and related to the corresponding

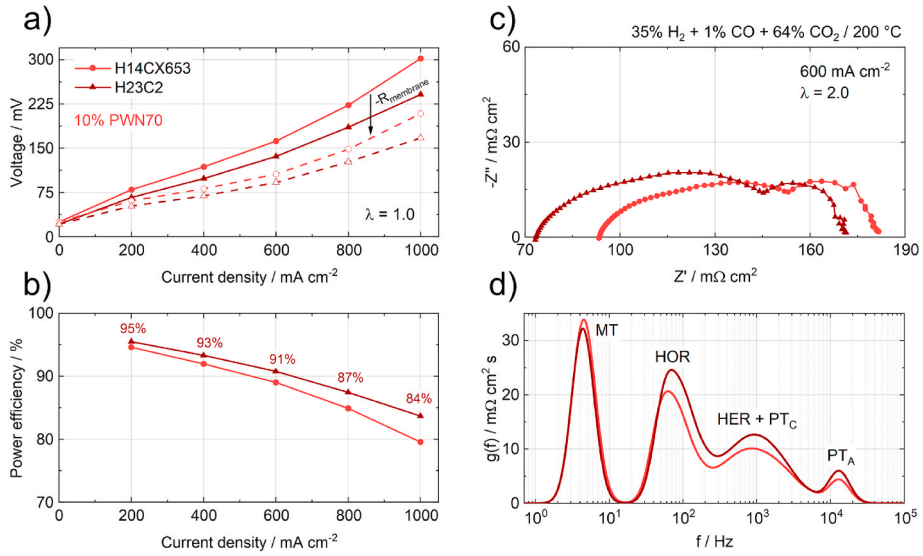

Fig. 9. a) EHP polarization curves with different GDEs and an identical CL containing 10 % PWN70 binder, b) the corresponding power efficiency, c) EIS spectra measured in the same cells at different stoichiometry, and d) the corresponding DRTs. The void symbols in a) represent the polarization curves corrected for the respective high-frequency resistance.

properties such as hydrophobicity, pore volume, and homogeneity of the respective catalyst layers.

Although PWN70 binder is relatively hydrophilic due to the high concentration of acidic groups, the corresponding CL provided excellent gas transport properties because of its superior porosity and the interaction of the ionomer with the PA. On the contrary, PPFSt-Imi produced electrodes with a lower porosity than those with PTFE binder. Adding the nonionic surfactant Triton X −100 to the PPFSt-Imi catalyst ink increased the pore volume and homogeneity of the respective CL. Subsequently, PPFSt-Imi binder also allowed efficient gas diffusion, further supported by the higher hydrophobicity of the corresponding CL, reducing the PA content in the electrodes. Additionally, all ionomers reduced the HER resistance significantly. Although the CLs fabricated with both ionomers exhibited very different properties, both outperformed the CL with the commonly employed PTFE binder.

The impact of two different GDLs on the EHP resistances was also investigated. The Freudenberg H23C2 GDL performed better than the Freudenberg H14CX653 GDL due to a better interfacial conductivity between the MEA components and facilitated gas diffusion. However, the H14CX653 GDL retained a higher PA content in the CL due to its higher MPL hydrophobicity, which improved the cell's proton transport and kinetics. Finally, a high power efficiency of 95 % at 0.2 A cm^{-2} with 100 % H_2 recovery was obtained.

CRediT authorship contribution statement

M. Braig: Writing – original draft, Visualization, Methodology, Investigation, Formal analysis, Data curation. **H. Cho:** Writing – review & editing, Methodology, Investigation, Formal analysis, Data curation. **C. Marchfelder:** Writing – review & editing, Investigation, Formal analysis, Data curation. **V. Atanasov:** Writing – review & editing, Supervision, Project administration, Investigation, Funding acquisition, Formal analysis, Data curation. **R. Zeis:** Writing – review & editing, Supervision, Project administration, Methodology, Investigation, Funding acquisition, Formal analysis, Conceptualization.

Declaration of competing interest

The authors declare that they have no known competing financial interests or personal relationships that could have appeared to influence the work reported in this paper.

Acknowledgements

The authors thank the ZSW (Zentrum für Sonnenenergie und Wasserstoff-Forschung) Ulm for providing the hydrogen test stations infrastructure. This work contributes to the research performed at CELEST (Center for Electrochemical Energy Storage Ulm-Karlsruhe).

References

[1] Huang F, Pingitore AT, Benicewicz BC. Electrochemical hydrogen separation from reformate using high-temperature polybenzimidazole (PBI) membranes: the role of chemistry. ACS Sustainable Chem Eng 2020;8:6234–42. https://doi.org/10.1021/acssuschemeng.9b07037.

[2] Pingitore AT, Huang F, Qian G, Benicewicz BC. Durable high polymer content m/p-Polybenzimidazole membranes for extended lifetime electrochemical devices. ACS Appl Energy Mater 2019;2:1720–6. https://doi.org/10.1021/acsaem.8b01820.

[3] Braig M, Zeis R. Distribution of relaxation times analysis of electrochemical hydrogen pump impedance spectra. J Power Sources 2023;576:233203. https://doi.org/10.1016/j.jpowsour.2023.233203.

[4] Mack F, Morawietz T, Hiesgen R, Kramer D, Gogel V, Zeis R. Influence of the polytetrafluoroethylene content on the performance of high-temperature polymer electrolyte membrane fuel cell electrodes. Int J Hydrogen Energy 2016;41:7475–83. https://doi.org/10.1016/j.ijhydene.2016.02.156.

[5] Mack F, Klages M, Scholta J, Jörissen L, Morawietz T, Hiesgen R, et al. Morphology studies on high-temperature polymer electrolyte membrane fuel cell electrodes. J Power Sources 2014;255:431–8. https://doi.org/10.1016/j.jpowsour.2014.01.032.

[6] Park JO, Kwon K, Cho MD, Hong S-G, Kim TY, Yoo DY. Role of binders in high temperature PEMFC electrode. J Electrochem Soc 2011;158:B675–81. https://doi.org/10.1149/1.3573773.

[7] Atanasov V, Lee AS, Park EJ, Maurya S, Baca ED, Fujimoto C, et al. Synergistically integrated phosphonated poly(pentafluorostyrene) for fuel cells. Nat Mater 2021;20:370–7. https://doi.org/10.1038/s41563-020-00841-z.

[8] Adhikari S, Leonard DP, Lim KH, Park EJ, Fujimoto C, Morales-Collazo O, et al. Hydrophobic quaternized poly(fluorene) ionomers for emerging fuel cells. ACS Appl Energy Mater 2022;5:2663–8. https://doi.org/10.1021/acsaem.2c00119.

[9] Kim YS. Hydrocarbon ionomeric binders for fuel cells and electrolyzers. Adv Sci 2023:1–32. https://doi.org/10.1002/advs.202303914. 2303914.

[10] Venugopalan G, Bhattacharya D, Andrews E, Briceno-Mena L, Romagnoli J, Flake J, et al. Electrochemical pumping for challenging hydrogen separations. ACS Energy Lett 2022;7:1322–9. https://doi.org/10.1021/acsenergylett.1c02853.

[11] Venugopalan G, Bhattacharya D, Kole S, Ysidron C, Angelopoulou PP, Sakellariou G, et al. Correlating high temperature thin film ionomer electrode binder properties to hydrogen pump polarization. Mater Adv 2021;2:4228–34. https://doi.org/10.1039/d1ma00208b.

[12] Ivers-Tiffée E, Weber A. Evaluation of electrochemical impedance spectra by the distribution of relaxation times. J Ceram Soc Japan 2017;125:193–201. https://doi.org/10.2109/jcersj2.16267.

[13] Braig M, Cho H, Marchfelder C, Atanasov V, Zeis R. Poly(pentafluorstyrene) based ionomers for electrochemical hydrogen pumps with 100% H2 recovery I – how

electrode properties affect the cell performance. Int J Hydrogen Energy 2025;174:151219. https://doi.org/10.1016/j.ijhydene.2025.151219.
[14] Cho H, Seiler J, Atanasova P, Atanasov V. Ion-pair membrane based on imidazolium-functionalized poly(pentafluorostyrene) for high-temperature proton exchange membrane fuel cell application. https://doi.org/10.1021/acsaem.3c02854; 2024.
[15] Heinzmann M, Weber A, Ivers-Tiffée E. Advanced impedance study of polymer electrolyte membrane single cells by means of distribution of relaxation times. J Power Sources 2018;402:24–33. https://doi.org/10.1016/j.jpowsour.2018.09.004.
[16] Liu H, Ney L, Zamel N, Li X. Effect of catalyst ink and formation process on the multiscale structure of catalyst layers in PEM fuel cells. Appl Sci 2022;12. https://doi.org/10.3390/app12083776.
[17] Song CH, Park JS. Effect of dispersion solvents in catalyst inks on the performance and durability of catalyst layers in proton exchange membrane fuel cells. Energies 2019;12. https://doi.org/10.3390/en12030549.
[18] Doo G, Lee JH, Yuk S, Choi S, Lee DH, Lee DW, et al. Tuning the ionomer distribution in the fuel cell catalyst layer with scaling the ionomer aggregate size in dispersion. ACS Appl Mater Interfaces 2018;10:17835–41. https://doi.org/10.1021/acsami.8b01751.
[19] Huang DC, Yu PJ, Liu FJ, Huang SL, Hsueh KL, Chen YC, et al. Effect of dispersion solvent in catalyst ink on proton exchange membrane fuel cell performance. Int J Electrochem Sci 2011;6:2551–65. https://doi.org/10.1016/s1452-3981(23)18202-2.
[20] Braig M, Deissler NH, Lüdeking I, Regnet F, Bevilacqua N, Zeis R. FIB-SEM and ToF-SIMS analysis of high-temperature PEM fuel cell electrodes. Adv Mater Interfac 2023;10. https://doi.org/10.1002/admi.202202430.
[21] Mack F, Gogel V, Jörissen L, Kerres J. Novel anode based on sulfonated polysulfone for medium temperature direct methanol fuel cells. J Power Sources 2013;239:651–8. https://doi.org/10.1016/j.jpowsour.2012.12.118.
[22] Lee WJ, Lee JS, Park HY, Park HS, Lee SY, Song KH, et al. Improvement of fuel cell performances through the enhanced dispersion of the PTFE binder in electrodes for use in high temperature polymer electrolyte membrane fuel cells. Int J Hydrogen Energy 2020;45:32825–33. https://doi.org/10.1016/j.ijhydene.2020.03.095.
[23] Lee AS, Choe YK, Matanovic I, Kim YS. The energetics of phosphoric acid interactions reveals a new acid loss mechanism. J Mater Chem A 2019;7:9867–76. https://doi.org/10.1039/c9ta01756a.
[24] Mack F, Heissler S, Laukenmann R, Zeis R. Phosphoric acid distribution and its impact on the performance of polybenzimidazole membranes. J Power Sources 2014;270:627–33. https://doi.org/10.1016/j.jpowsour.2014.06.171.
[25] Korte C. Phosphoric acid, an electrolyte for fuel cells - temperature and composition dependence of vapor pressure and proton conductivity. Fuel Cell Sci Eng Mater Process Syst Technol 2012;1:335–59. https://doi.org/10.1002/9783527650248.ch12.
[26] Melchior JP, Kreuer KD, Maier J. Proton conduction mechanisms in the phosphoric acid-water system (H4P2O7-H3PO4·2H2O): a 1H, 31P and 17O PFG-NMR and conductivity study. Phys Chem Chem Phys 2017;19:587–600. https://doi.org/10.1039/c6cp04855b.
[27] Heinzmann M, Weber A, Ivers-Tiffée E. Impedance modelling of porous electrode structures in polymer electrolyte membrane fuel cells. J Power Sources 2019;444. https://doi.org/10.1016/j.jpowsour.2019.227279.
[28] Eikerling M, Kornyshev AA. Electrochemical impedance of the cathode catalyst layer in polymer electrolyte fuel cells. J Electroanal Chem 1999;475:107–23.
[29] Lee KS, Spendelow JS, Choe YK, Fujimoto C, Kim YS. An operationally flexible fuel cell based on Quaternary ammonium-biphosphate ion pairs. Nat Energy 2016;1. https://doi.org/10.1038/nenergy.2016.120.
[30] Lim KH, Matanovic I, Maurya S, Kim Y, De Castro ES, Jang JH, et al. High temperature polymer electrolyte membrane fuel cells with high phosphoric acid retention. ACS Energy Lett 2023;8:529–36. https://doi.org/10.1021/acsenergylett.2c02367.
[31] Kannan A, Li Q, Cleemann LN, Jensen JO. Acid distribution and durability of HT-PEM fuel cells with different electrode supports. Fuel Cells 2018;18:103–12. https://doi.org/10.1002/fuce.201700181.
[32] Bevilacqua N, George MG, Bazylak A, Zeis R. Phosphoric acid distribution patterns in high temperature PEM fuel cells. ECS Trans 2017;80:409. https://doi.org/10.1149/08008.0409ecst.
[33] Wong AKC, Banerjee R, Bazylak A. Tuning MPL intrusion to increase oxygen transport in dry and partially saturated polymer electrolyte membrane fuel cell gas diffusion layers. J Electrochem Soc 2019;166:F3009–19. https://doi.org/10.1149/2.0021907jes.
[34] Freudenberg Performance Materials SE & Co. KG. Freudenberg gas diffusion layer - fuel cell technical data. 2021.